Emittance Preservation Through Density Ramp Matching Sections in a Plasma Wakefield Accelerator

Yujian Zhao,[1] Weiming An,[2, 1, *] Xinlu Xu,[1, 3, †] Fei Li,[1] Lance Hildebrand,[1]
Mark J. Hogan,[3] Vitaly Yakimenko,[3] Chan Joshi,[4] and Warren B. Mori[1, 4]

[1] *Department of Physics and Astronomy, University of California Los Angeles, Los Angeles, CA 90095, USA*
[2] *Department of Astronomy, Beijing Normal University, Beijing 100875, China*
[3] *SLAC National Accelerator Laboratory, Menlo Park, California 94025, USA*
[4] *Department of Electrical Engineering, University of California Los Angeles, Los Angeles, CA 90095, USA*
(Dated: May 24, 2020)

In plasma wakefield acceleration, the witness beam's emittance needs to be preserved when it propagates through a plasma stage. The plasma includes density ramps at both the entrance and the exit. Using the WKB solution of a single particle's motion, analytical expressions for the evolution of the beam emittance and the Twiss parameters in an arbitrary adiabatic plasma profile are provided neglecting the acceleration of the beam inside the plasma. It is shown that the beam emittance can be preserved under the matching condition even when the beam has an initial energy spread. It is also shown that the emittance growth for an unmatched beam is minimized when it is focused to the same vacuum plane for a matched beam. The emittance evolution from 3D QuickPIC simulation results agree well with the theoretical results. In the some of the proposed experiments on nearly completed FACET II facility, the matching condition may not be perfectly satisfied and the wake may not be perfectly symmetric. It is shown that for a given set of beam parameters that are consistent with FACET II capabilities, even when the assumptions of the theory are not satisfied, the emittance growth can still be minimized by choosing the optimal focal plane. Last, another issue that may cause emittance growth in realistic plasmas is also examined. When using a lithium plasma source in FACET II experiments a helium buffer gas is used. The plasma is formed from field ionization which can lead to a nonlinear focusing force when there are nonuniform helium ions due to its high ionization potential. For an initial beam emittance of 20μm, the helium ionization is found to be small and the witness beam's emittance can be preserved.

I. INTRODUCTION

During the past two decades of research, a number of impressive advances have been made in the beam-driven Plasma Wakefield Acceleration (PWFA) concept. For instance, experiments have shown that these wakes can sustain accelerating gradients exceeding 50 GeV/m over $\sim$ meter in length [1], and the acceleration of the witness beam in PWFA can be highly efficient while maintaining a high acceleration gradient and small energy spread [2]. In PWFA, an ultra-relativistic electron beam (the drive beam) is used to form a plasma wake that accelerates a second electron beam (the witness beam) that is properly loaded inside the wake. In the so-called blowout regime, the drive beam density is much higher than the plasma density. The electric field of the drive beam will expel all the plasma electrons away and leave an ion channel (i.e. a bubble) after it. As shown in Fig. 1, when the witness beam is located at a proper position inside the wake, the accelerating field can be flattened in order to preserve the energy spread. At the back of the bubble, where the witness beam is located, not only is there a longitudinal electric field that provides a high acceleration gradient, but there is also a transverse focusing force. In addition, when there is azimuthal symmetry, in these nonlin-
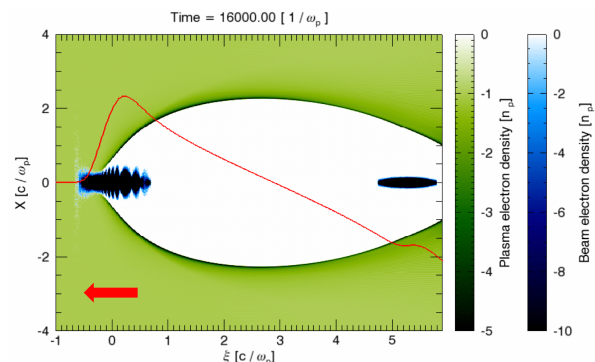

FIG. 1. A snapshot of the drive and witness beam of a sample simulation of a two bunch PWFA. A data is in the $x - \xi$ plane at $y = 0$. Both beams (blue) are propagating to the left. The green area shows the unperturbed plasma electron density, the white area is the uniform plasma ions (ion channel/bubble). The red curve is the lineout of the accelerating field E_z on the axis (in arbitrary units).

ear wakes the longitudinal electric field (the accelerating field) does not depend on r and the transverse focusing force is linear (proportional to r), points radially inward, and does not depend on $\xi = ct - z$ inside the bubble [3]. The fact that the accelerating field does not depend on r ensures that the beam particles will not gain additional slice energy spread when undergoing acceleration and betatron oscillations inside the bubble. Furthermore,

the fact that the transverse linear focusing force does not depend on ξ ensures that the beam particles at different longitudinal positions will oscillate at the same betatron frequency, if they have the same energy. If one of these properties is satisfied then the Panofsky Wenzel theorem [4, 5] guarantees that the other is as well.

When the beam has no energy spread, its emittance is conserved under a linear focusing force inside the symmetric bubble. When the beam has an energy spread, and/or there is acceleration with imperfect beam loading (particles at different longitudinal positions in the beam feel a different accelerating field, E_z), the beam's emittance may increase during its propagation in the plasma. The topic of emittance growth and preservation is very important and is being actively studied [6–13].

Recently, expressions for emittance evolution in uniform plasma, both for cases when the beam does [10] or does not have [11] longitudinal acceleration have been published. It has also been shown that several plasma density profiles provide exact solutions to single particle motion [10, 12], therefore the evolution of the beam's Twiss parameters can be calculated and used to match the beam into a plasma. In this paper, we investigate how the emittance grows when a beam is not matched in an adiabatic plasma ramp. In complimentary work, R. Ariniello et al. [13] have recently shown that if a beam is matched to an adiabatic plasma profile, the emittance will oscillate around its initial value with a small amplitude (10^{-4} times the initial emittance) for a 2% energy spread(and the amplitude of oscillations scales as σ_γ^2).

In typical experiments (e.g. the FACET II experiments at SLAC [14]), the plasma density profile is usually fixed with density ramps at the entrance and the exit. Therefore the beam parameters need to be optimized to match the beam to the plasma. It has been shown that if the witness beam is initially matched to the plasma, its emittance can be preserved very well [14]. However, if the witness beam parameters are fixed, it usually cannot be perfectly matched to an arbitrary plasma density ramp. In this paper, we investigate the witness beam's emittance evolution in this situation. We first derive an analytical expression for the beam's emittance evolution in an arbitrary adiabatic plasma profile, assuming the beam has no longitudinal acceleration. This analytical expression can be used to predict the emittance growth when the beam has an energy spread and is not initially matched. This analysis is complimentary to that in [13] where it was assumed that the beam was nearly matched and the emittance growth was small. We also discuss how to choose the relative focal plane by either moving the plasma or the focal position of the beam to minimize the emittance growth for an unmatched beam with fixed parameters. It is found that the beam emittance growth can be minimized when choosing the focal plane to be the vacuum focus for a beam that was matched. Another issue that may cause emittance growth in recently proposed energy doubling of the witness beam experiment at FACET II experiments [1] is the ionization of helium

buffer gas when using the Lithium plasma source. Additional self-ionization [15] by the beam can modify the focusing fields in the buffer region. In the last section, we show that under that situation the emittance growth is due to the nonlinear focusing force felt by the beam, which is caused by the nonuniform helium ion density in the plasma. The helium ionization can be minimized by using a 20 μm initial emittance witness bunch. Therefore such a bunch can be propagated while gaining energy without measurable emittance growth.

II. THEORETICAL ANALYSIS OF EMITTANCE EVOLUTION IN ARBITRARY ADIABATIC PLASMA DENSITY PROFILE

In the blowout regime of PWFA with the assumption of azimuthal symmetry (we will henceforth use this assumption), the focusing force felt by an electron in the witness beam is $\mathbf{F}_\perp = -m_e\omega_p^2\mathbf{r}/2$ (where m_e is the electron mass, $\omega_p = \sqrt{\frac{n_p e^2}{\epsilon_0 m_e}}$ is the plasma frequency, n_p is the plasma density, ϵ_0 is the vacuum permittivity, e is the elementary charge), which is proportional to the radial distance r and independent of $\xi = ct - z$. Therefore the motions of the beam particle in x and y directions are decoupled, and we will only study the beam particle motion in the x direction. If we assume a beam particle's energy is a constant, the equation of motion for this particle is

$$x''(z) + k_\beta(z)^2 x(z) = 0 \tag{1}$$

where z is the coordinate along the direction of propagation, $k_\beta(z) = \frac{\omega_p(z)}{\sqrt{2\gamma}c}$, $\omega_p(z)$ is the plasma frequency at position z, γ is the relativistic factor of the beam particle, c is the speed of light. In a uniform plasma, $\omega_p(z)$ is a constant, so the solution to equation (1) is a simple harmonic oscillation. With a given initial phase space distribution for the beam, we can obtain an analytical expression for the emittance evolution[10, 11]. For nonuniform plasma, there is no general analytical solution to equation (1). However, as long as the plasma density is changing adiabatically, i.e.,

$$\frac{|k_\beta'(z)|\frac{2\pi}{k_\beta(z)}}{k_\beta(z)} \ll 1 \tag{2}$$

or

$$\frac{\pi}{k_\beta(z)n_p(z)}\left|\frac{dn_p(z)}{dz}\right| \ll 1$$

we can use WKB method [16] to get an approximate solution to equation (1), and calculate the emittance evolution with the WKB solution.

The WKB solution to equation (1) is:

$$x(z) = x(0)\frac{\sqrt{\beta_m(z)}}{\sqrt{\beta_m(0)}}\cos[\phi(z)]$$
$$+ \sqrt{\beta_m(z)\beta_m(0)}\Big[x'(0) + \frac{\alpha_m(0)}{\beta_m(0)}x(0)\Big]\sin[\phi(z)] \quad (3)$$

where

$$\beta_m(z) = 1/k_\beta(z), \quad \alpha_m(z) = -\frac{1}{2}\frac{d\beta_m(z)}{dz} \quad (4)$$

are the Twiss parameters for a single particle in an adiabatically changing profile, and $\phi(z) = \int_0^z k_\beta(s)ds$ is the phase advance. $x(0)$ and $x'(0)$ are the initial values for the beam particle. Then the adiabatic condition (2) can be simplified to [13]

$$|\alpha_m(z)| \ll 1 \quad (5)$$

We note that if the plasma density profile is $n_p(z) = \frac{n_{p0}}{(1+z/l)^4}$ (where l is a constant), then equation (1) has an exact solution [12], which is the same as its WKB solution described in equation (3).

For brevity, we henceforth denote $x(z)$ by x, $x(0)$ by x_i, $\beta_m(z)$ by β_m, $\beta_m(0)$ by β_{mi}, $\alpha_m(z)$ by α_m, $\alpha_m(0)$ by α_{mi}, $\phi(z)$ by ϕ. From (3) and its derivative, we can obtain

$$\begin{pmatrix} x \\ x' \end{pmatrix} = M \begin{pmatrix} x_i \\ x'_i \end{pmatrix} = \begin{pmatrix} M_{11} & M_{12} \\ M_{21} & M_{22} \end{pmatrix} \begin{pmatrix} x_i \\ x'_i \end{pmatrix}$$

where M is the transport matrix and

$$M_{11} = \sqrt{\frac{\beta_m}{\beta_{mi}}}(\cos\phi + \alpha_{mi}\sin\phi)$$
$$M_{12} = \sqrt{\beta_m\beta_{mi}}\sin\phi$$
$$M_{21} = \frac{(\alpha_{mi} - \alpha_m)\cos\phi - (1 + \alpha_{mi}\alpha_m)\sin\phi}{\sqrt{\beta_m\beta_{mi}}}$$
$$M_{22} = \sqrt{\frac{\beta_{mi}}{\beta_m}}(\cos\phi - \alpha_m\sin\phi)$$

The geometric emittance is defined as

$$\epsilon = \sqrt{\langle x^2\rangle\langle x'^2\rangle - \langle xx'\rangle^2} \quad (6)$$

where $\langle\rangle$ is the ensemble average. It then follows that (see Appendix A for details)

$$\langle x^2\rangle = \langle(M_{11}x_i + M_{12}x'_i)^2\rangle$$
$$= \epsilon_i\beta_m(A + B_1C + B_2S), \quad (7)$$

where:

$$A = \frac{\beta_i\gamma_{mi} + \gamma_i\beta_{mi} - 2\alpha_i\alpha_{mi}}{2},$$
$$B_1 = \frac{\beta_i}{\beta_{mi}} - A = \frac{\beta_i}{\beta_{mi}} - \frac{\beta_i\gamma_{mi} + \gamma_i\beta_{mi} - 2\alpha_i\alpha_{mi}}{2},$$
$$B_2 = \frac{\beta_i}{\beta_{mi}}\alpha_{mi} - \alpha_i,$$
$$C = \int d\phi f_\phi(\phi)\cos 2\phi,$$
$$S = \int d\phi f_\phi(\phi)\sin 2\phi,$$

and $\epsilon_i = \sqrt{\langle x_i^2\rangle\langle x_i'^2\rangle - \langle x_ix_i'\rangle^2}$, $\beta_i = \langle x_i^2\rangle/\epsilon_i$, $\gamma_i = \langle x_i'^2\rangle/\epsilon_i$, $\alpha_i = -\langle x_ix_i'\rangle/\epsilon_i$ are the beam's initial geometric emittance and Twiss parameters, $\gamma_m = (1+\alpha_m^2)/\beta_m$, and $f_\phi(\phi)$ is the distribution function for the beam particles' phase advance. For a beam with no energy spread, $f_\phi(\phi) = \delta(\phi - \phi_0)$ where $\phi_0 = \int_0^z k_\beta(s)ds = \int_0^z \frac{\omega_p(s)}{\sqrt{2\gamma}c}ds$.

We can also obtain

$$\langle x'^2\rangle = \epsilon_i\Big[A\gamma_m + \frac{-B_1 - 2B_2\alpha_m + B_1\alpha_m^2}{\beta_m}C$$
$$+ \frac{-B_2 + 2B_1\alpha_m + B_2\alpha_m^2}{\beta_m}S\Big] \quad (8)$$

and

$$\langle xx'\rangle = -\epsilon_i[A\alpha_m + (B_1\alpha_m - B_2)C + (B_2\alpha_m + B_1)S] \quad (9)$$

Using equations (7)-(9), and noting that A, B_1 and B_2 satisfy $B_1^2 + B_2^2 = A^2 - 1$, we can obtain an analytical expression of emittance growth for arbitrary $f_\phi(\phi)$ with small energy spread

$$\epsilon = \sqrt{\langle x^2\rangle\langle x'^2\rangle - \langle xx'\rangle^2}$$
$$= \epsilon_i\sqrt{A^2 - (A^2 - 1)(C^2 + S^2)} \quad (10)$$

Denote the average relativistic factor of the beam as $\bar{\gamma}$. When the relative energy spread of the beam is very small (i.e. for every particle $|\Delta\gamma| = |\gamma - \bar{\gamma}| \ll \bar{\gamma}$), the particle's phase advance in the plasma ϕ will become $\phi(\gamma) = \bar{\phi} - \frac{\bar{\phi}}{2\bar{\gamma}}\Delta\gamma$, where $\bar{\phi} = \phi(\bar{\gamma})$ (See Appendix C for details). Assuming a Gaussian energy distribution, for the beam particles we have:

$$f_\gamma(\gamma) = \frac{1}{\sqrt{2\pi}\sigma_\gamma}\exp[-\frac{(\gamma - \bar{\gamma})^2}{2\sigma_\gamma^2}]$$

As a result, ϕ will also have a Gaussian distribution

$$f_\phi(\phi) = \frac{1}{\sqrt{2\pi}\sigma_\phi}\exp[-\frac{(\phi - \bar{\phi})^2}{2\sigma_\phi^2}]$$

where

$$\sigma_\phi = \frac{\bar{\phi}}{2}\frac{\sigma_\gamma}{\bar{\gamma}} \qquad (11)$$

$\frac{\sigma_\gamma}{\bar{\gamma}}$ is the relative energy spread of the beam. With this Gaussian distribution of ϕ, we can obtain:

$$C = \exp(-2\sigma_\phi^2)\cos(2\bar{\phi}), \quad S = \exp(-2\sigma_\phi^2)\sin(2\bar{\phi}) \quad (12)$$

Inserting (12) into (10) and using (11), we get an analytical expression of emittance growth for a beam that has a Gaussian energy distribution with a small energy spread:

$$\frac{\epsilon}{\epsilon_i} = A\sqrt{1 - \frac{A^2-1}{A^2}\exp[-(\frac{\sigma_\gamma}{\bar{\gamma}}\bar{\phi})^2]} \qquad (13)$$

where $\frac{\sigma_\gamma}{\bar{\gamma}}$ is the energy spread, and $\bar{\phi} = \frac{1}{\sqrt{2}\bar{\gamma}c}\int_0^z \omega_p(s)ds$ is the phase change of an electron with energy $\bar{\gamma}$ after it propagates for a longitudinal distance of z inside the plasma. Because we assume the beam's energy, $\bar{\gamma}$, does not change, then

$$\frac{\epsilon}{\epsilon_i} = \frac{\bar{\gamma}\epsilon}{\bar{\gamma}\epsilon_i} \approx \frac{\epsilon_n}{\epsilon_{ni}}$$

where $\epsilon_n = \frac{1}{m_e c}\sqrt{\langle x^2\rangle\langle p_x^2\rangle - \langle xp_x\rangle^2}$ is the normalized emittance and p_x is the transverse momentum of the particle. This means the normalized emittance growth is approximately the same as the geometric emittance growth. Note that in order to keep the analysis tractable we have only kept the effects of the energy spread in the betatron phase advance and not on the amplitude of the betatron oscillation in the elements of the transport matrix. The amplitudes are functions of the local values of the Twiss parameters while the phase is an integral in z over $1/\beta_m$. Therefore, only the phase terms can deviate substantially between particles with small energy differences. Thus, the small amplitude oscillation of the emittance seen in Ref. [13] when a matched beam has finite energy spread is absent here.

In Fig. 2, we compare the theoretical results from (13) with QuickPIC [17, 18] simulation results. We choose a plasma density profile $n_p(z) = \frac{n_{p0}}{(1+z/l)^2}$, for which the adiabatic condition is independent of z. In the simulation, we turn off the longitudinal acceleration for the beam particles (i.e. the energy of the beam particle essentially does not change), and choose reasonable parameters to make the simulation in the blowout regime. Fig. 2(a) shows that when the beam is initially matched, the beam's emittance is a constant during its propagation inside the plasma. As shown in Fig. 2(b)(c)(d), if the beam is not initially matched, the theoretical results based on the WKB solution agree with the simulation result very well.

Note that in (13), $A \geqslant 1$ is always true (see the Appendix B). So $\epsilon/\epsilon_i \leqslant A$. When the beam propagates in
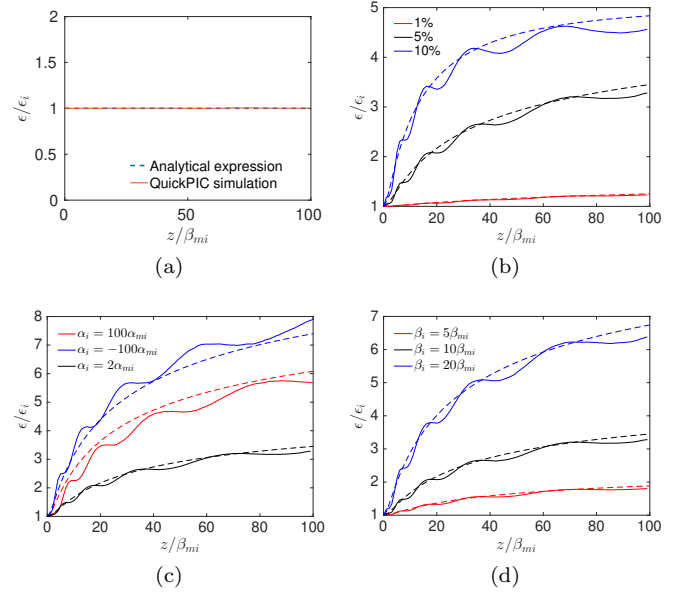

FIG. 2. Emittance evolution in plasma ramp: $n_p(z) = \frac{n_{p0}}{(1+z/l)^2}$ ($l = 5$, l and z are normalized to β_{mi}). For (a) the beam is initially matched: $\beta_i = \beta_{mi}$, $\alpha_i = \alpha_{mi} = -\frac{1}{2l} = -0.1$, and the beam has a 5% energy spread. For (b) the beam is initially unmatched: $\beta_i = 10\beta_{mi}$, $\alpha_i = 2\alpha_{mi}$, and the beam has 1%, 5%, 10% initial energy spreads respectively. For (c) the beam is initially unmatched: $\beta_i = 10\beta_{mi}$, $\alpha_i = 2\alpha_{mi}, 100\alpha_{mi}, -100\alpha_{mi}$ respectively, and the beam has a 5% energy spread. For (d) the beam is initially unmatched: $\alpha_i = 2\alpha_{mi}$, $\beta_i = 5\beta_{mi}, 10\beta_{mi}, 20\beta_{mi}$ respectively, and the beam has a 5% energy spread. In (b)(c)(d), the solid lines are from QuickPIC simulations, and the dashed lines are from the analytical expression (13). In these three plots, the solid black lines correspond to the same simulation result, and the dashed black lines correspond to the same analytical expression.

the plasma for a very long distance, $\bar{\phi}$ will become very large, and the beam will have a saturated emittance:

$$\frac{\epsilon_{sat}}{\epsilon_i} = A = \frac{\beta_i\gamma_{mi} + \gamma_i\beta_{mi} - 2\alpha_i\alpha_{mi}}{2} \qquad (14)$$

For the special case when the plasma is uniform along z, we have $\alpha_m = \alpha_{mi} = 0$, so $\gamma_m = \gamma_{mi} = 1/\beta_{mi}$, then

$$A = \frac{\gamma_i\beta_{mi} + \beta_i/\beta_{mi}}{2}$$

Therefore, the emittance growth in a longitudinally uniform plasma will be

$$\frac{\epsilon}{\epsilon_i} = \frac{\gamma_i\beta_{mi} + \beta_i/\beta_{mi}}{2} \times$$
$$\sqrt{1 - \frac{(\gamma_i\beta_{mi} + \beta_i/\beta_{mi})^2 - 4}{(\gamma_i\beta_{mi} + \beta_i/\beta_{mi})^2}\exp[-(\frac{\sigma_\gamma}{\bar{\gamma}}\bar{\phi})^2]} \qquad (15)$$

which is mathematically equivalent to equation (7) in [11], and similar to equation (1) in [10] (difference is due to the different assumptions for $f_\phi(\phi)$).

We define the beam to be initially matched when

$$\alpha_i = \alpha_{mi}, \ \beta_i = \beta_{mi}, \ \gamma_i = \gamma_{mi} \qquad (16)$$

Then we have $A = 1, B_1 = 0, B_2 = 0$. Therefore, from equations (7) - (9) and (13), we have $\langle x^2 \rangle / \epsilon_i = \beta_m$, $\langle x'^2 \rangle / \epsilon_i = \gamma_m$, $-\langle xx' \rangle / \epsilon_i = \alpha_m$ and $\epsilon = \epsilon_i$. So $\beta = \langle x^2 \rangle / \epsilon = \beta_m$, $\gamma = \langle x'^2 \rangle / \epsilon = \gamma_{mi}$, $\alpha = -\langle xx' \rangle / \epsilon = \alpha_m$. Therefore, with an adiabatic plasma density profile, when neglecting the beam's energy change, if the beam is initially matched, the beam's Twiss parameters along z will be $\beta_m, \gamma_m, \alpha_m$, and the beam's geometric emittance will not change. We can therefore interpret β_m, α_m defined in (4) and γ_m as the matched Twiss parameters.

If the beam's initial Twiss parameters deviate from the matched ones, i.e.,

$$\alpha_i = \alpha_{mi} + \Delta\alpha, \ \beta_i = \beta_{mi} + \Delta\beta$$

where $|\Delta\alpha| \ll 1$ and $|\Delta\beta|/\beta_{mi} \ll 1$, then

$$A \approx 1 + \frac{1}{2}\Delta\alpha^2 + \frac{\gamma_{mi}}{2\beta_{mi}}\Delta\beta^2 - \frac{\alpha_{mi}}{\beta_{mi}}\Delta\alpha\Delta\beta \qquad (17)$$

Inserting this into (13) gives

$$\frac{\epsilon}{\epsilon_i} \approx 1 + (\frac{1}{2}\Delta\alpha^2 + \frac{\gamma_{mi}}{2\beta_{mi}}\Delta\beta^2 - \frac{\alpha_{mi}}{\beta_{mi}}\Delta\alpha\Delta\beta)[1 - e^{-(\frac{\sigma_\gamma}{\bar{\gamma}}\bar{\phi})^2}]$$

We can also get the expression for β from the above equations. Inserting (12) into (7) and using (11) leads to

$$\langle x^2 \rangle = \epsilon_i \beta_m \left\{ A + \left[B_1 \cos(2\bar{\phi}) + B_2 \sin(2\bar{\phi}) \right] e^{-\frac{1}{2}(\frac{\sigma_\gamma}{\bar{\gamma}}\bar{\phi})^2} \right\}$$

Dividing both sides by ϵ and using (13) gives

$$\beta = \beta_m \frac{A + \left[B_1 \cos(2\bar{\phi}) + B_2 \sin(2\bar{\phi}) \right] \exp[-\frac{1}{2}(\frac{\sigma_\gamma}{\bar{\gamma}}\bar{\phi})^2]}{A\sqrt{1 - \frac{A^2-1}{A^2}\exp[-(\frac{\sigma_\gamma}{\bar{\gamma}}\bar{\phi})^2]}} \qquad (18)$$

If there is no energy spread ($\sigma_\gamma = 0$), this equation can be simplified

$$\beta = \beta_m \left[A + B_1 \cos(2\phi) + B_2 \sin(2\phi) \right] \qquad (19)$$

which is similar in form to equation (11) in [13] but with different coefficients.

III. ON MINIMIZING THE EMITTANCE GROWTH FOR A FIXED BEAM

In the previous section, it was shown that the beam emittance will be preserved as long as the beam satisfies the matching condition (equation (16)). In this case $\beta^* = 1/\gamma_{mi}$ (β^* is β when $\alpha = 0$) which we define as the matched β^*, β_m^*. It was also shown how the emittance grows if the beam is slightly mismatched as might be the case if there are shot to shot variations of the beam and/or plasma conditions. In addition, in a controlled experiment that might for example be conducted

at FACET II [14], the beam emittance and optics are relatively fixed so that β^* can be assume to be fixed. However, for a given plasma profile the plasma conditions at the plasma entrance are such that it will not be possible to match a beam with a given β^* (i.e. $\beta^* \neq \beta_m^*$). It is therefore useful to determine the best location to focus such a beam. This is defined to be the focal position in vacuum ($z = s$) that minimizes the emittance growth for a given beam and plasma profile, assuming the plasma entrance is at $z = 0$.

Therefore,

$$\alpha(s) = 0, \ \beta(s) = \beta^*$$

where β^* is β at the focal plane. According to the evolution of Twiss parameters in a drift space [19], the beam's initial Twiss parameters at the plasma entrance ($z = 0$) are

$$\alpha_i = \alpha(0) = \frac{s}{\beta^*}, \ \beta_i = \beta(0) = \beta^* + \frac{s^2}{\beta^*}, \ \gamma_i = \gamma(0) = \frac{1}{\beta^*} \qquad (20)$$

Using equation (13), we can calculate the emittance growth using the above initial condition, and find the optimal s defined to be when $d\epsilon/ds = 0$. For a fixed plasma density profile, $d\epsilon/ds = 0$ reduces to $dA/ds = 0$, which gives us the optimal s,

$$s_o = \frac{\alpha_{mi}}{\gamma_{mi}} \qquad (21)$$

This optimal $s = s_o$ is actually the focal position in vacuum for the matched beam (whose initial Twiss parameters at the plasma entrance are α_{mi}, β_{mi} and γ_{mi}). In other words, by putting the unmatched beam's focal plane at the same position as the matched beam's focal plane in vacuum, the unmatched beam will have minimal emittance growth in the plasma. We can calculate this minimal emittance growth by evaluating A using the initial Twiss parameters from (20) and (21), giving $A = A_o \equiv \frac{1}{2}(\beta^* \gamma_{mi} + \frac{1}{\beta^* \gamma_{mi}})$. We then insert this into (13) to get the minimal emittance growth.

If the witness beam's focal plane in vacuum deviates from the the optimal position (21): $s = s_o + \Delta s$, from (20) and (21) we can obtain:

$$A = A_o + \frac{\gamma_{mi}}{2\beta^*}\Delta s^2$$

We can see that for $s = s_o + \Delta s$ and $s = s_o - \Delta s$, the corresponding A are the same, so according to (13), the emittance growth are the same as well. In other words, the emittance growth as a function of s is symmetric about $s = s_o$.

If we assume Δs is a small quantity, then for a fixed z we get,

$$\frac{\epsilon}{\epsilon_i} \approx \frac{\epsilon_o}{\epsilon_i} + \left\{ 1 - \exp[-(\frac{\sigma_\gamma}{\bar{\gamma}}\bar{\phi})^2] \right\} \frac{A_o}{\epsilon_o/\epsilon_i} \frac{\gamma_{mi}}{2\beta^*}\Delta s^2$$

where $\epsilon_o \equiv \epsilon(A_o)$ is the emittance when $\Delta s = 0$ (or $s = s_o$).

This analysis also permits examining how the shot to shot variance of the plasma density at the entrance of the profile affects the emittance growth (essentially A), assuming the beam profile and the position of the plasma entrance (β^* and s) are fixed. From equation (14) and the relation $\gamma_{mi} = (1 + \alpha_{mi}^2)/\beta_{mi}$, we have

$$A = \frac{\beta_i(1 + \alpha_{mi}^2)/\beta_{mi} + \gamma_i\beta_{mi} - 2\alpha_i\alpha_{mi}}{2}$$

Since we assume the beam profile and the position of the plasma entrance are fixed, from equation (20) we know α_i, β_i, γ_i are fixed. The shot to shot changes to the plasma profile lead to the variances of α_{mi} and β_{mi}, which leads to the first order variance of A:

$$\delta A_1 = \frac{\partial A}{\partial \alpha_{mi}}\delta\alpha_{mi} + \frac{\partial A}{\partial \beta_{mi}}\delta\beta_{mi}$$
$$= (\frac{\beta_i}{\beta_{mi}}\alpha_{mi} - \alpha_i)\delta\alpha_{mi} + \frac{1}{2}(\gamma_i - \gamma_{mi}\frac{\beta_i}{\beta_{mi}})\delta\beta_{mi}$$

$$\tag{22}$$

Especially, we can see that at the matching point, the variance of α_{mi} and β_{mi} will not cause the variance of A to the first order. The second order variation of A is

$$\delta A_2 = \frac{1}{2}\delta\alpha_{mi}^2 + \frac{\gamma_{mi}}{2\beta_{mi}}\delta\beta_{mi}^2 - \frac{\alpha_{mi}}{\beta_{mi}}\delta\alpha_{mi}\delta\beta_{mi}$$

which is consistent with equation (17). Essentially, variations can arise from either the plasma profile or beam profile at the plasma entrance.

Next we carry out some QuickPIC simulations using plasma and beam parameters that are close to the ones in the proposed FACET II experiment, while satisfying all the theoretical assumptions (adiabatic plasma profile, azimuthal symmetry in plasma wake, etc). We turn off the longitudinal push in the simulation so that the beam has no longitudinal acceleration. The plasma density profile we use is shown in Fig. 3(b). This profile is the region between 5 cm and 75 cm of the full profile (Fig. 3(a)). The adiabatic condition ($|\alpha_m| < 1$) is now satisfied throughout the entire profile. At the entrance and exit $|\alpha_m| = 0.24$ and 0.56 respectively. In addition, $\alpha_{mi} = 0.24$, $\beta_{mi} = 0.0194$ m for the simulation. The theory could be easily modified to include a matching section [10] or a perturbative section as in [13]. We use a non-evolving symmetric drive beam to create a well formed ion bubble, and the witness beam is the same as the one in FACET II (See Table I and II). Fig. 4 shows the simulation results and the good agreement between the simulations and the theory. It also shows that the expression for emittance growth in a uniform plasma (equation (15)) cannot describe the emittance growth in an adiabatic plasma precisely.
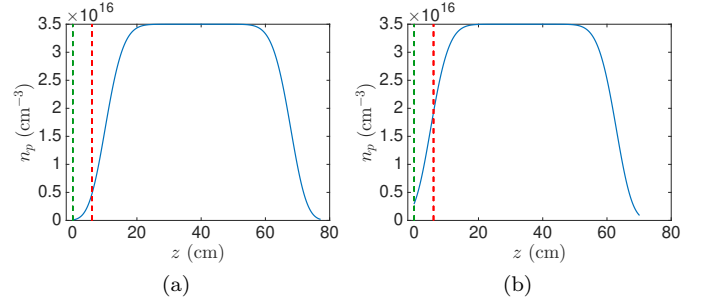

(a)

(b)

FIG. 3. Plasma density profile. The green dashed line is the entrance of the plasma, and the red dashed line is the position of the witness beam's focal plane in vacuum. The beams propagate to the right in the plot. (a) The FACET II plasma density profile. (b) The profile used for the simulation results in Fig. 4. Only the region between 5 cm and 75 cm of the profile in (a) is used. In this region the adiabatic condition is always satisfied.
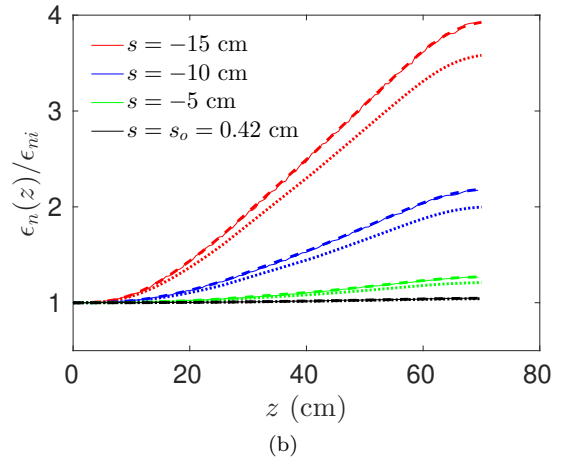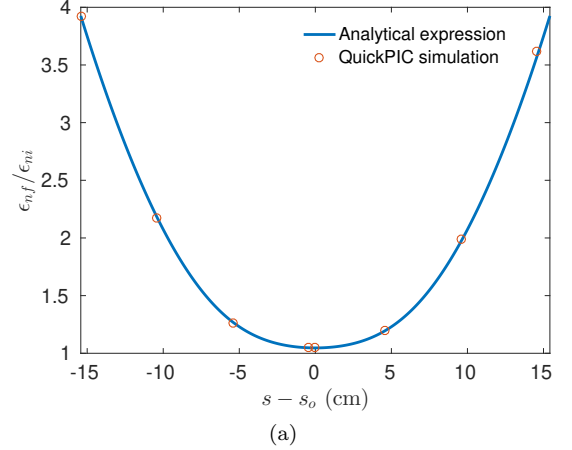

(a)

(b)

FIG. 4. Witness beam's emittance growth for different focal planes, s, in the adiabatic plasma in Fig. 3(b). (a) The ratio of final emittance (at the plasma exit) to the initial emittance (at the plasma entrance) for different cases. (b) The evolution of ϵ_n inside the plasma for 4 different cases, corresponding to the 4 orange spots for $s - s_o \leq 0$ in (a). The solid lines are from QuickPIC simulations, the dashed lines are from expression (13), and the dotted lines are from expression (15).

IV. EMITTANCE EVOLUTION IN PREFORMED PLASMA USING FACET II PARAMETERS

Table I shows a possible set of beams parameters for the two-bunch FACET II experiments.

	Energy(GeV)	Q(nC)	$\sigma_z(\mu m)$	$\epsilon_{n_x}(\mu m)$	$\epsilon_{n_y}(\mu m)$
Drive	10	1.6	6.4	3.4	3.0
Witness	10	0.5	5.0	3.15	3.15

TABLE I. Possible beam parameters for two-bunch PWFA experiment at FACET II

	α_x	α_y	$\beta_x(m)$	$\beta_y(m)$
Drive Beam	59	12	127	27
Witness Beam	40	40	80	80

TABLE II. The Twiss parameters of both beams at the exit of the final focusing magnet.

Both beams are tri-Gaussian with $n_b = \frac{N}{(2\pi)^{\frac{3}{2}}} e^{-\frac{x^2}{2\sigma_x^2}} e^{-\frac{y^2}{2\sigma_y^2}} e^{-\frac{z^2}{2\sigma_z^2}}$. The σ_z is the rms pulse length for the beam, and ϵ_{n_x} and ϵ_{n_y} are the normalized emittance in x, y directions respectively. The distance between the drive and witness beam is 150 μm. The initial relative rms energy spread for both beams is 0.25%. Table II shows the Twiss parameters for both beams at the exit of the final focusing magnet. Note that in this setup the drive beam is asymmetric and the witness beam is symmetric, so the wake felt by the witness beam is not azimuthally symmetric.

The plasma density profile in the simulation is shown in the Fig. 3(a), which is close to the plasma density profile of the lithium source used in the FACET II experiment. The peak plasma density is 3.5×10^{16}cm^{-3}, which is chosen to ensure that the witness beam is located inside the bubble wake at a position that flattens the accelerating field (as shown in Fig. 1).

With such a plasma density profile, the initial matched Twiss parameters for the witness beam at the plasma entrance are:

$$\alpha_{mi} = 0.916, \ \beta_{mi} = 0.068\text{m} \qquad (23)$$

These parameters are not calculated directly from (4) at $z = 0$ because the plasma near the entrance does not satisfy the adiabatic condition (5). Instead, they are obtained by neglecting any energy spread, and integrating the following equation (See appendix D for derivation) for β,

$$\frac{1}{2}\beta(z)\beta''(z) - \frac{1}{4}\beta'(z)^2 + \beta(z)^2 k_\beta(z)^2 = 1 \ , \alpha(z) = -\frac{1}{2}\beta'(z) \qquad (24)$$

from the flat-topped region of the plasma back to the entrance of the plasma with initial Twiss parameters $\beta = \sqrt{2\overline{\gamma}}\frac{c}{\omega_p}$, $\alpha = 0$ (where ω_p is the plasma frequency for the flat-topped plasma) [14]. According to the matched parameters given in (23), the optimal s for the plasma density profile can be calculated from (21), $s = s_o = 3.39$ cm. Fig. 5 shows the evolution of β for the real witness beam when its focal plane in vacuum is located at a different $s = s_o + \Delta s$. The solid red line is the case if the

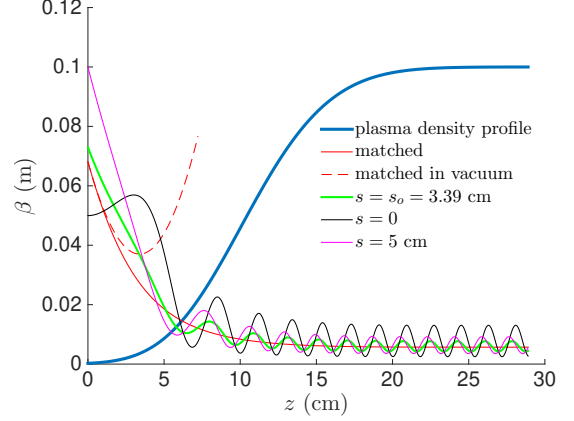FIG. 5. The evolution of β for the witness beam for different s from numerical calculation. The plasma density profile is in arbitrary units.

witness beam was initially matched to the plasma profile. We can see that for a matched beam β evolves smoothly and stays constant in the uniform plasma region while for an unmatched beam the beam's β will oscillate.

Next, we run QuickPIC simulations in which we vary s but with the same beams as described in Table I and II. This time we turn on the longitudinal push in the simulation so the witness beam is gaining energy. Fig. 6(a) shows the normalized emittance growth at the exit of the plasma when the witness beam's focal plane in vacuum is located at $s = $ -10, -5, 0, 3.39, 5, 10, 15, 20 cm (note that negative s means the focal plane of the witness beam is outside the plasma). We can clearly see that the optimal s for minimizing the emittance growth is at $s = 3.39$ cm. This illustrates that experiments can be performed at FACET II that provide easily measurable differences in the emittance growth as the focal point is changed.

We note that the different emittance growth in x and y directions is caused by the asymmetry of the drive beam, which excites asymmetric wakefields that have different linear focusing forces in x and y directions [20]. We note that even though the plasma and the beam parameters used in these simulations don't satisfy the assumptions we made in the previous sections (the drive beam is asymmetric and the plasma near the entrance and the exit is not adiabatic), (21) still appears to predict the optimal focal position of the witness beam very well, although the initial matched Twiss parameters α_{mi}, β_{mi} are calculated in a different way. Fig. 6(b) shows the evolution
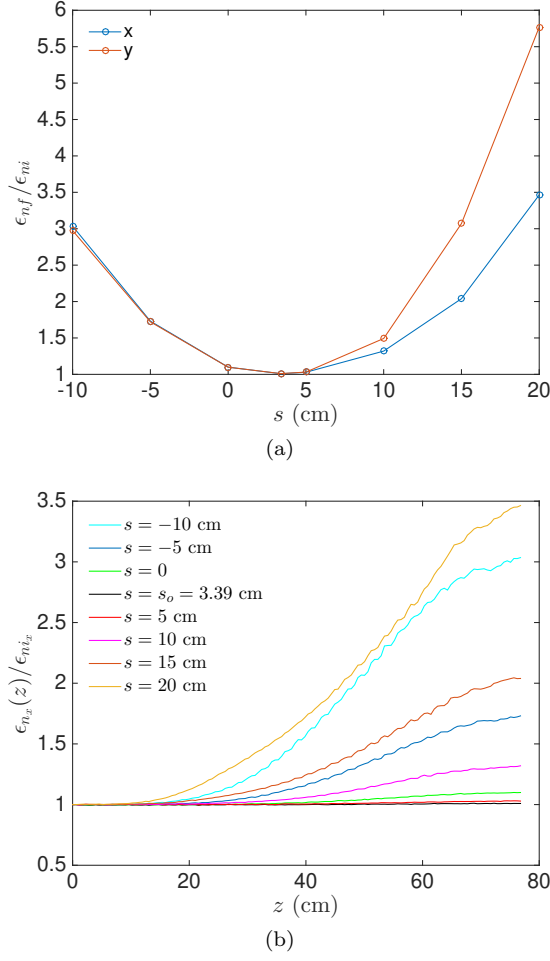
(a)

(b)

FIG. 6. The normalized emittance growth of the witness beam for different s. (a) The ratio of final emittance (at the plasma exit) to the initial emittance (at the plasma entrance) for different cases. (b) The evolution of ϵ_{n_x} inside the plasma for different cases, corresponding to the blue line in (a).

of witness beam's ϵ_{n_x} along z. We can see that when $s = 3.39$ cm, ϵ_{n_x} is almost preserved although the beam is not initially matched.

V. EMITTANCE EVOLUTION IN LITHIUM PLASMA WITH HELIUM BUFFER GAS

In FACET II experiments, lithium will be one of the choices for the plasma source. The hot lithium vapor will be confined and cooled at each end by the helium buffer gas [1, 2]. The plasma is generated by the intense electric field of the drive/witness beams when they pass through and ionize the lithium vapor. In the previous section, we simulated the beams evolving in a preformed and radially uniform plasma. In this section, we use QuickPIC to simulate the emittance evolution when the plasma is self-formed by field ionization of a neutral gas from the intense electric field of the drive and witness beams. Fig. 7 shows the profile for the lithium gas and the helium
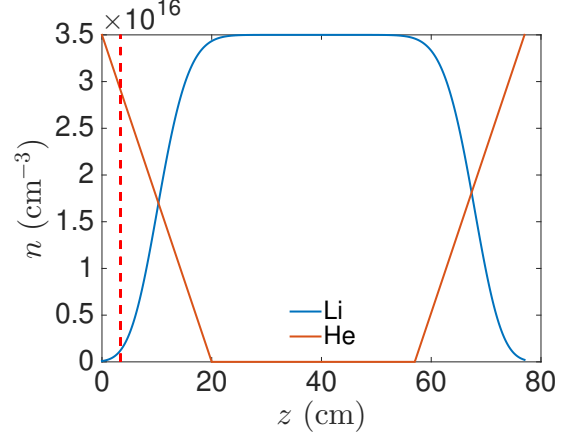
buffer gas in our simulation.

FIG. 7. Helium and lithium gas density profile. The red dashed line is the position of the witness beam's focal plane: $z = 3.39$ cm

The blue line in Fig. 7 is the lithium gas density, which is the same as the profile shown in Fig. 3(a) in the previous section. There are two linear helium ramps (orange line in Fig. 7) at the entrance and exit of the lithium gas. The beam parameters are the same as described in the previous section, and we choose the optimal value $s = 3.39$ cm for the witness beam's focal position in vacuum. Fig. 8(a) shows the witness beam's emittance evolution inside the plasma. We can see that in the beginning and the end of the simulation, emittance growth occurs. In the middle of the lithium region where there is no helium, the emittance essentially stays the same.
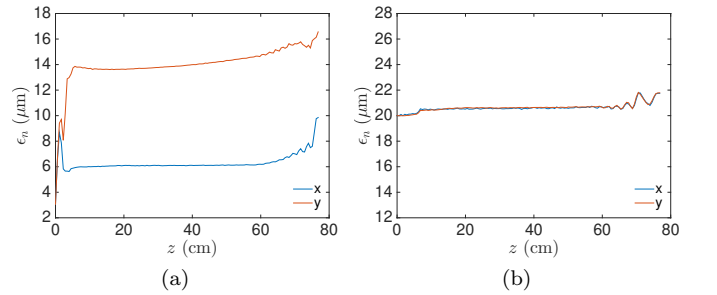

(a)

(b)

FIG. 8. The evolution of normalized emittance of the witness beam: (a) We use the same parameters as we used in the preformed plasma simulation in the previous section: Drive beam: $\epsilon_{n_x} = 3.4$ μm, $\epsilon_{n_y} = 3.0$ μm, witness beam: $\epsilon_{n_x} = \epsilon_{n_y} = 3.15$ μm. (b) We increase the initial emittance for both beams to 20 μm (in both x and y directions).

The reason for the large emittance growth is that the beams can ionize the helium buffer gas which results in a nonlinear focusing force inside the bubble. Fig. 9(a) shows the helium ion density snapshot when the beams propagate for 1 cm in the plasma. The drive beam's center is located at $\xi = -5.27$, and the witness beam's center is located at $\xi = 0$. Both beams are propagating

from right to left. The drive beam enters the plasma with a larger spot size than the witness beam, so it can only ionize a part of the neutral helium while the witness beam can ionize most of the neutral helium around it. Fig. 9(b) shows the focusing fields felt by the witness beam at different ξ at the same propagation distance as Fig. 9(a). The focusing fields felt by the witness beam is no longer linear when helium is ionized by itself. Therefore, the witness beam has a large emittance growth in the region where the helium gas is ionized. In the region where there is only lithium, the witness beam will still feel a linear focusing force and its emittance only grows because the witness beam is no longer matched in the uniform region of lithium plasma, which causes a much smaller growth than that from the region where helium gas exists.
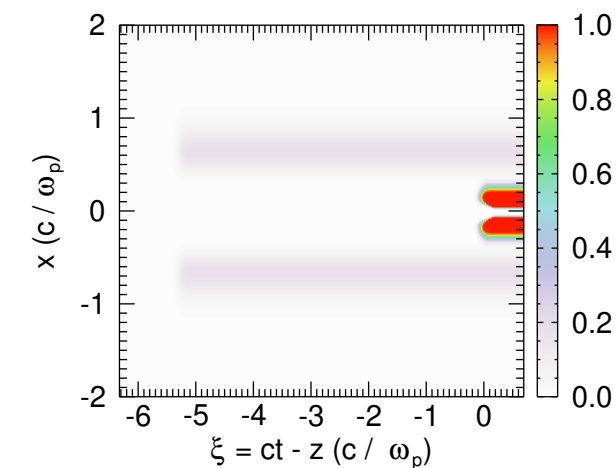
(a)
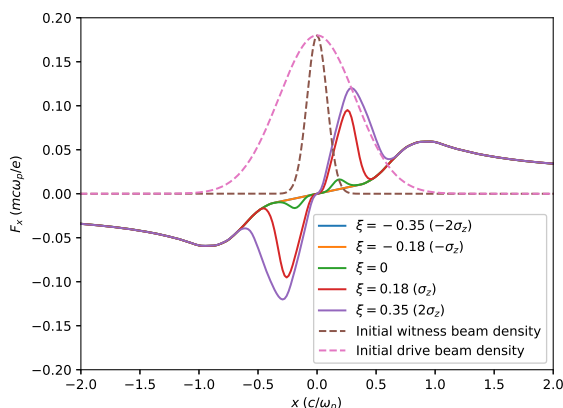
(b)

FIG. 9. (a) Helium ion charge density. The grey area is the helium ions produced by the drive beam, and the red area is the helium ions produced by the witness beam. (b) The F_x transverse lineouts at different longitudinal positions, ξ, and the initial beam density profiles (in arbitrary units).

In order to avoid the emittance growth in the lithium plasma source, we can increase the initial emittances for both the drive beam and witness beam. In Fig. 8(b), we show the QuickPIC simulation results when using an initial beam emittance of 20 μm while keeping the other parameters the same as the simulation shown in Fig. 8(a). When the initial beam emittance becomes larger, the initial spot sizes of both beams will increase, and the Coulomb field around the beam will become smaller. Therefore, when the beams pass through the helium buffer gas, the neutral helium is weakly ionized. However, the lithium can still be ionized and form the plasma wake because lithium has a lower ionization energy than helium. When there is no helium ionization, the focusing force felt by the witness beam is linear, and its emittance barely grows, as shown in Fig. 8(b). The small emittance growth at the exit of the plasma in Fig. 8(b) is still caused by the helium ionization because the witness beam enters into the exit ramp of helium with a smaller spot size compared to its initial spot size at the entrance of the plasma.

VI. CONCLUSION

We have used theory and QuickPIC simulations to examine the evolution of the emittance and the Twiss parameters of particle beams in plasmas whose density is changing adiabatically. We use the WKB solution for each particle and assume the energy of each particle in the beam does not change to obtain an analytical expression for the beam's emittance evolution in an arbitrary adiabatic plasma density profile in a nonlinear PWFA. When the beam has no initial energy spread, its emittance will remain a constant in the azimuthally symmetric blowout regime. When there is an initial energy spread, the beam's emittance can be preserved as long as its initial Twiss parameters are matched to the density profile of the plasma ramp. We also use this expression to analyze the emittance growth when the position of the witness beam's focal plane in vacuum is changed while keeping the beam parameters and the plasma density profile fixed. When the beam cannot be matched, the emittance growth can be minimized by focusing the unmatched beam to the same vacuum focal plane position as the matched beam. We used QuickPIC simulations for possible FACET II beam parameters to show that the emittance can indeed be preserved very well when we choose the focal plane position to be the same as for a matched beam, even when the assumptions of symmetric blowout and adiabatic density evolution for the entire plasma region are not satisfied. For other focal plane positions, the witness beam's emittance is larger at the exit of the plasma.

In addition, we also examined through simulations the effect of additional self-ionization of the buffer gas by the drive beam. At FACET II a lithium gas is confined by a helium buffer gas. When the drive and/or witness beam

emittance is small (around 3 μm), they can be focused to small enough spot sizes so that they can ionize the helium buffer gas. This will lead to the focusing fields felt by the witness beam to be strongly nonlinear. We find that this can potentially lead to the witness beam's emittance growing by a factor of 3 and 5 in the x and y planes respectively for sample FACET II parameters. The different growth in x and y directions is caused by the asymmetry of the drive beam forming an asymmetric plasma wake. By using an initial emittance of 20 μm, the helium buffer gas is weakly ionized and the witness beam's emittance can be preserved very well.

Appendix A: Calculation of beam moment $\langle x^2 \rangle$

In this appendix we provide details on calculating the second moment of the beam, i.e., the square of the spot-size.

$$
\begin{aligned}
\langle x^2 \rangle &= \int x^2 f(x, x') dx dx' \\
&= \int x^2 f_i(x_i, x_i') dx_i dx_i' \\
&= \int (M_{11} x_i + M_{12} x_i')^2 f_i(x_i, x_i') dx_i dx_i'
\end{aligned}
$$

where $f(x, x')$ is the distribution function at z and f_i is the initial distribution function. From the Vlasov equation we have $f(x, x') = f_i(x_i, x_i')$, and $dx dx' = dx_i dx_i'$ because $\det(M) = 1$.

The last step above is correct only if all the particles have the same energy. However, since different particles have different energy γ, their corresponding transport matrices M are different. In order to calculate the above integral with an energy spread in the beam, we assume the main difference in M is the phase advance ϕ. Even though the β_m, α_m in M are different (because of different γ), we assume them to be the same for all the particles and use $\gamma = \bar{\gamma}$ ($\bar{\gamma}$ is the mean energy among all the particles), while claiming the main difference is in ϕ due to different energy γ. After the beam propagates for a distance z, we denote the distribution of the phase advance ϕ as $f_\phi(\phi)$ (with the normalization $\int f_\phi(\phi) d\phi = 1$). So:

$$
\begin{aligned}
\langle x^2 \rangle &= \iiint (M_{11} x_i + M_{12} x_i')^2 f(x_i, x_i') f_\phi(\phi) dx_i dx_i' d\phi \\
&= \langle x_i^2 \rangle \int d\phi f_\phi(\phi) M_{11}^2 + \langle x_i'^2 \rangle \int d\phi f_\phi(\phi) M_{12}^2 \\
&\quad + \langle x_i x_i' \rangle \int d\phi f_\phi(\phi) 2 M_{11} M_{12} \\
&= \epsilon_i \Big[\beta_i \int d\phi f_\phi(\phi) M_{11}^2 + \gamma_i \int d\phi f_\phi(\phi) M_{12}^2 \\
&\quad - \alpha_i \int d\phi f_\phi(\phi) 2 M_{11} M_{12} \Big]
\end{aligned}
$$
(A1)

where

$$
\begin{aligned}
&\int d\phi f_\phi(\phi) M_{11}^2 \\
&= \frac{\beta_m}{\beta_{mi}} \int d\phi f_\phi(\phi) (\cos\phi + \alpha_{mi} \sin\phi)^2 \\
&= \frac{1}{2} \frac{\beta_m}{\beta_{mi}} [(1 + C) + \alpha_{mi}^2 (1 - C) + 2\alpha_{mi} S] \\
&= \frac{1}{2} \frac{\beta_m}{\beta_{mi}} [\beta_{mi} \gamma_{mi} + (1 - \alpha_{mi}^2) C + 2\alpha_{mi} S]
\end{aligned}
$$

$$
\begin{aligned}
&\int d\phi f_\phi(\phi) M_{12}^2 \\
&= \beta_m \beta_{mi} \int d\phi f_\phi(\phi) \sin^2\phi \\
&= \frac{1}{2} \beta_m \beta_{mi} (1 - C)
\end{aligned}
$$
(A2)

$$
\begin{aligned}
&\int d\phi f_\phi(\phi) 2 M_{11} M_{12} \\
&= \beta_m \int d\phi f_\phi(\phi) (2\cos\phi \sin\phi + 2\alpha_{mi} \sin^2\phi) \\
&= \beta_m [S + \alpha_{mi}(1 - C)]
\end{aligned}
$$

and where

$$
C = \int d\phi f_\phi(\phi) \cos 2\phi, \quad S = \int d\phi f_\phi(\phi) \sin 2\phi \quad (A3)
$$

Finally, we obtain:

$$
\begin{aligned}
\langle x^2 \rangle = \epsilon_i \beta_m \Big[&\frac{\beta_i \gamma_{mi} + \gamma_i \beta_{mi} - 2\alpha_i \alpha_{mi}}{2} \\
&+ \Big(\frac{\beta_i}{\beta_{mi}} - \frac{\beta_i \gamma_{mi} + \gamma_i \beta_{mi} + 2\alpha_i \alpha_{mi}}{2} \Big) C \\
&+ \Big(\frac{\beta_i}{\beta_{mi}} \alpha_{mi} - \alpha_i \Big) S \Big]
\end{aligned}
$$
(A4)

We can define:

$$
\begin{aligned}
A &= \frac{\beta_i \gamma_{mi} + \gamma_i \beta_{mi} - 2\alpha_i \alpha_{mi}}{2} \\
B_1 &= \frac{\beta_i}{\beta_{mi}} - A = \frac{\beta_i}{\beta_{mi}} - \frac{\beta_i \gamma_{mi} + \gamma_i \beta_{mi} - 2\alpha_i \alpha_{mi}}{2} \\
B_2 &= \frac{\beta_i}{\beta_{mi}} \alpha_{mi} - \alpha_i
\end{aligned}
$$
(A5)

Leading to:

$$
\langle x^2 \rangle = \epsilon_i \beta_m (A + B_1 C + B_2 S) \quad (A6)
$$

Appendix B: Proof of $A \geqslant 1$

$$
\begin{aligned}
A &= \frac{\beta_i \gamma_{mi} + \gamma_i \beta_{mi} - 2\alpha_i \alpha_{mi}}{2} \\
&\geqslant \frac{2\sqrt{\beta_i \gamma_{mi} \gamma_i \beta_{mi}} - 2\alpha_i \alpha_{mi}}{2} \\
&= \sqrt{(1+\alpha_i^2)(1+\alpha_{mi}^2)} - \alpha_i \alpha_{mi} \\
&= \sqrt{1 + \alpha_i^2 + \alpha_{mi}^2 + \alpha_i^2 \alpha_{mi}^2} - \alpha_i \alpha_{mi} \\
&\geqslant \sqrt{1 + 2\alpha_i \alpha_{mi} + \alpha_i^2 \alpha_{mi}^2} - \alpha_i \alpha_{mi} \\
&= |1 + \alpha_i \alpha_{mi}| - \alpha_i \alpha_{mi} \\
&\geqslant 1
\end{aligned}
\tag{B1}
$$

Appendix C

In this appendix we derive the first order correction to the phase advance due to variation of the energy of the particle. We begin with the definition for the phase

$$
\phi = \int_0^z \frac{\omega_p(s)}{\sqrt{2\gamma}c} ds
$$

Due to the variation of γ, the variation of ϕ is

$$
\begin{aligned}
\Delta\phi &= \Delta \int_0^z \frac{\omega_p(s)}{\sqrt{2\gamma}c} ds \\
&= \int_0^z \Delta\left(\frac{\omega_p(s)}{\sqrt{2\gamma}c}\right) ds \\
&= \int_0^z -\frac{1}{2}\left(\frac{\omega_p(s)}{\sqrt{2}\gamma^{\frac{3}{2}}c}\right)\Delta\gamma\, ds \\
&= -\frac{\Delta\gamma}{2\gamma} \int_0^z \frac{\omega_p(s)}{\sqrt{2\gamma}c} ds \\
&= -\frac{\phi}{2\gamma}\Delta\gamma
\end{aligned}
\tag{C1}
$$

So the difference between the phase advance of a particle with energy γ and the phase advance of a particle with

the average energy $\bar{\gamma}$ is

$$
\phi(\gamma) - \phi(\bar{\gamma}) = -\frac{\phi(\bar{\gamma})}{2\bar{\gamma}}\Delta\gamma
\tag{C2}
$$

and

$$
\phi(\gamma) = \bar{\phi} - \frac{\bar{\phi}}{2\bar{\gamma}}\Delta\gamma
\tag{C3}
$$

Appendix D: Differential equation for β

In this appendix, we offer a derivation of equation (24) in the text. We start from the definition of the beam's spot size:

$$
\sigma_x = \sqrt{\langle x^2 \rangle}
$$

Taking derivatives with respect to z provide:

$$
\sigma_x' = \frac{\langle xx' \rangle}{\sigma_x}
$$

$$
\sigma_x'' = \frac{\langle x^2 \rangle \langle x'^2 \rangle - \langle xx' \rangle^2}{\sigma_x^3} + \frac{\langle xx'' \rangle}{\sigma_x}
$$

Using the definition of geometric emittance (6) and the equation of motion (1), leads to:

$$
\sigma_x'' = \frac{\epsilon^2}{\sigma_x^3} - k_\beta^2 \sigma_x
$$

If we assume the beam has no energy spread, then under a linear focusing force, the beam's normalized emittance ϵ_n is a constant, so $\epsilon = \epsilon_n/\gamma$ is also a constant. Finally, if we use the definition of β: $\beta = \frac{\sigma_x^2}{\epsilon}$, we obtain

$$
\frac{1}{2}\beta\beta'' - \frac{1}{4}\beta'^2 + \beta^2 k_\beta^2 = 1
$$

ACKNOWLEDGMENTS

[1] I. Blumenfeld, C. Clayton, F.-J. Decker, M. Hogan, C.-K. Huang, R. Ischebeck, R. Iverson, C. Joshi, T. Katsouleas, N. Kirby, W. Lu, K. Marsh, W. Mori, P. Muggli, E. Oz, R. Siemann, D. Walz, and M. Zhou, Energy doubling of 42 gev electrons in a metre-scale plasma wakefield accel-

erator, Nature **445**, 741 (2007).
[2] M. Litos, E. Adli, W. An, C. Clarke, C. Clayton, S. Corde, D. jean pierre, R. England, A. Fisher, J. Frederico, S. Gessner, S. Green, M. Hogan, C. Joshi, W. Lu, K. Marsh, W. Mori, P. Muggli, N. Vafaei-Najafabadi,

and G. Yocky, High-efficiency acceleration of an electron beam in a plasma wakefield accelerator, Nature **515**, 92 (2014).

[3] W. Lu, C. Huang, M. Zhou, W. B. Mori, and T. Katsouleas, Nonlinear theory for relativistic plasma wakefields in the blowout regime, Phys. Rev. Lett. **96**, 165002 (2006).

[4] W. K. H. Panofsky and W. A. Wenzel, Some considerations concerning the transverse deflection of charged particles in radio-frequency fields, Review of Scientific Instruments **27**, 967 (1956).

[5] P. B. Wilson, Introduction to wakefields and wake potentials, AIP Conference Proceedings **184**, 525 (1989).

[6] T. Mehrling, J. Grebenyuk, F. S. Tsung, K. Floettmann, and J. Osterhoff, Transverse emittance growth in staged laser-wakefield acceleration, Phys. Rev. ST Accel. Beams **15**, 111303 (2012).

[7] I. Dornmair, K. Floettmann, and A. R. Maier, Emittance conservation by tailored focusing profiles in a plasma accelerator, Phys. Rev. ST Accel. Beams **18**, 041302 (2015).

[8] P. Antici, A. Bacci, C. Benedetti, E. Chiadroni, M. Ferrario, A. R. Rossi, L. Lancia, M. Migliorati, A. Mostacci, L. Palumbo, and L. Serafini, Laser-driven electron beamlines generated by coupling laser-plasma sources with conventional transport systems, Journal of Applied Physics **112**, 044902 (2012).

[9] M. Migliorati, A. Bacci, C. Benedetti, E. Chiadroni, M. Ferrario, A. Mostacci, L. Palumbo, A. R. Rossi, L. Serafini, and P. Antici, Intrinsic normalized emittance growth in laser-driven electron accelerators, Phys. Rev. ST Accel. Beams **16**, 011302 (2013).

[10] X. L. Xu, J. F. Hua, Y. P. Wu, C. J. Zhang, F. Li, Y. Wan, C.-H. Pai, W. Lu, W. An, P. Yu, M. J. Hogan, C. Joshi, and W. B. Mori, Physics of phase space matching for staging plasma and traditional accelerator components using longitudinally tailored plasma profiles, Phys. Rev. Lett. **116**, 124801 (2016).

[11] A. Aschikhin, T. J. Mehrling, A. M. de la Ossa, and J. Osterhoff, Analytical model for the uncorrelated emittance evolution of externally injected beams in plasma-based accelerators, Nuclear Instruments and Methods in Physics Research Section A: Accelerators, Spectrometers, Detectors and Associated Equipment **909**, 414 (2018), 3rd European Advanced Accelerator Concepts workshop (EAAC2017).

[12] K. Floettmann, Adiabatic matching section for plasma accelerated beams, Phys. Rev. ST Accel. Beams **17**, 054402 (2014).

[13] R. Ariniello, C. Doss, K. Hunt-Stone, J. Cary, and M. Litos, Transverse beam dynamics in a plasma density ramp, Physical Review Accelerators and Beams **22**, 10.1103/PhysRevAccelBeams.22.041304 (2019).

[14] C. Joshi, E. Adli, W. An, C. E. Clayton, S. Corde, S. Gessner, M. J. Hogan, M. Litos, W. Lu, K. A. Marsh, W. B. Mori, N. Vafaei-Najafabadi, B. O'shea, X. Xu, G. White, and V. Yakimenko, Plasma wakefield acceleration experiments at facet ii, Plasma Physics and Controlled Fusion **60**, 034001 (2018).

[15] D. L. Bruhwiler, D. A. Dimitrov, J. R. Cary, E. Esarey, W. Leemans, and R. E. Giacone, Particle-in-cell simulations of tunneling ionization effects in plasma-based accelerators, Physics of Plasmas **10**, 2022 (2003).

[16] D. J. Griffiths, *Introduction to Quantum Mechanics*.

[17] C. Huang, V. Decyk, C. Ren, M. Zhou, W. Lu, W. Mori, J. Cooley, T. Antonsen, and T. Katsouleas, Quickpic: A highly efficient particle-in-cell code for modeling wakefield acceleration in plasmas, Journal of Computational Physics **217**, 658 (2006).

[18] W. An, V. K. Decyk, W. B. Mori, and T. M. Antonsen, An improved iteration loop for the three dimensional quasi-static particle-in-cell algorithm: Quickpic, Journal of Computational Physics **250**, 165 (2013).

[19] S. Y. Lee, *Accelerator Physics*, 2nd ed. (World Scientific Publishing Co. Pte. Ltd, 2004).

[20] L. Hildebrand, W. An, X. Xu, F. Li, Y. Zhao, M. J. Hogan, V. Yakimenko, S. S. Nagaitsev, E. Adli, C. Joshi, and W. Mori, Mitigation techniques for witness beam hosing in plasma - based acceleration, 2018 IEEE Advanced Accelerator Concepts Workshop (AAC) **00**, 1 (2018).